Calhoun

Institutional Archive of the Naval Postgraduate School

Calhoun: The NPS Institutional Archive

Faculty and Researcher Publications   Faculty and Researcher Publications

2009

Tropical cyclone spin up revisited

Smith, R. K

Tropical cyclone spin-up revisited

Roger K. Smith[a]*, Michael T. Montgomery[b,c]† and Nguyen Van Sang[a]

[a] *Meteorological Institute, University of Munich, Germany*
[b] *Dept. of Meteorology, Naval Postgraduate School, Monterey, California, USA*
[c] *NOAA Hurricane Research Division, Miami, Florida, USA*

ABSTRACT: We present numerical experiments to investigate axisymmetric interpretations of tropical cyclone spin-up in a three-dimensional model. Two mechanisms are identified for the spin-up of the mean tangential circulation. The first involves the convergence of absolute angular momentum above the boundary layer and is a mechanism to spin up the outer circulation, i.e. to increase the vortex size. The second involves the convergence of absolute angular momentum within the boundary layer and is a mechanism to spin up the inner core. It is associated with the development of supergradient wind speeds in the boundary layer. The existence of these two mechanisms provides a plausible physical explanation for certain long-standing observations of typhoons by Weatherford and Gray, which indicate that inner-core changes in the azimuthal-mean tangential wind speed often occur independently from those in the outer core. The unbalanced dynamics in the inner-core region are important in determining the maximum radial and tangential flow speeds that can be attained, and therefore important in determining the azimuthal-mean intensity of the vortex. We illustrate the importance of unbalanced flow in the boundary layer with a simple thought experiment. The analyses and interpretations presented are novel and support a recent hypothesis of the boundary layer in the inner-core region. Copyright © 2009 Royal Meteorological Society

1. Introduction

This is one of a series of papers investigating tropical cyclone amplification in a three-dimensional model. In the first paper (Nguyen *et al.*, 2008; henceforth M1), we studied tropical cyclone intensification and predictability in the context of an idealized three-dimensional numerical model on an f-plane. The model has relatively basic physics including a bulk-aerodynamic formulation of the boundary layer and a simple explicit moisture scheme to represent deep convection. In the prototype amplification problem beginning with a weak tropical storm strength vortex, the emergent flow becomes highly asymmetric and dominated by deep convective vortex structures, even though the problem as posed is essentially axisymmetric. Following Hendricks *et al.* (2004) and Montgomery *et al.* (2006a), we refer to these structures as 'vortical hot towers' (VHTs). The VHTs amplify the local vertical vorticity of the rotation-rich environment of the incipient vortex. The evidence from the three papers above is that they are the basic coherent structures in the intensification process. In the numerical experiments it is the progressive segregation, merger and axisymmetrization of these towers and the low-level convergence they generate that

is fundamental to the intensification process, but axisymmetrization is never complete.

It was shown in M1 that the vortex asymmetries that develop are highly sensitive to the boundary-layer moisture distribution. When a small random moisture perturbation is added in the boundary layer at the initial time, the pattern of evolution of the flow asymmetries is dramatically changed and a non-negligible spread in the local and azimuthally averaged intensity results. Thus the intensification process is not only intrinsically asymmetric, but small-scale features thereof are random in nature.

Prior to our study, most theoretical paradigms for tropical cyclone intensification have been based on axisymmetric reasoning. One of these is the so-called WISHE mechanism, which is summarized by Emanuel *et al.* (1994) and further discussed by Craig and Gray (1996). The theory is articulated in a revised form by Montgomery *et al.* (2009; henceforth M2). The term WISHE, which stands for wind-induced surface heat exchange, was first coined by Yano and Emanuel (1991) to denote the source of fluctuations in subcloud-layer entropy arising from fluctuations in surface wind speed. The WISHE mechanism has become the accepted paradigm for explaining tropical cyclone dynamics and has achieved widespread acceptance in tropical weather briefings, in dynamic meteorology textbooks (e.g. Holton, 2004; Asnani, 2005), and in the current literature (Lighthill, 1998; Smith, 2003; Molinari *et al.*, 2004; Montgomery *et al.*, 2006a). It is central also to the theory for the potential intensity of tropical cyclones proposed by Emanuel

---

Correspondence to: Roger K. Smith, Meteorological Institute, University of Munich, Theresienstrasse 37, 80333 Munich, Germany. Email: roger.smith@lmu.de

†The contribution of Michael T. Montgomery to this article was prepared as part of his official duties as a United States Federal Government employee.

(1988). (See also Emanuel, 1995; Bister and Emanuel, 1998; Emanuel, 2003)

Recently, Smith *et al.* (2008) showed that a major deficiency of Emanuel's potential intensity theory is the tacit assumption of gradient wind balance in the boundary layer[†], a shallow layer in which inflow arises largely because of *gradient wind imbalance* in the radial momentum equation. If a more complete boundary layer formulation is included, the tangential wind speed in the boundary layer becomes supergradient in the inner-core region. Boundary layer calculations by Smith and Vogl (2008) suggest that supergradient flow is a ubiquitous feature of the inner-core boundary layer of a mature storm, a finding supported by the boundary layer calculations of Shapiro (1983), Kepert (2001), Kepert and Wang (2001) and Montgomery *et al.* (2001) and by the numerical model calculations of Nguyen *et al.* (2002).

Smith *et al.* (2008) proposed a revised model for the behaviour of the boundary layer in the inner-core region and its influence on the interior circulation as sketched in Figure 1. The boundary layer is divided into two regions depending on whether the top of the boundary layer is an inflow boundary (Region B, $r > r_{up}$) or an outflow boundary (Region A, $r < r_{up}$), where r denotes the radius. In Region B, the boundary layer is directly influenced by the vortex above through the radial pressure gradient at the top of the layer and through the downward advection of free vortex properties such as moisture, heat and momentum (e.g. Smith and Vogl, 2008). Except, of course, in regions of deep convection, such as rainbands, or indeed secondary eyewalls (Houze *et al.*, 2007; Terwey and Montgomery, 2008), there is no essential feedback to the free vortex. However, in Region A, boundary-layer properties are advected vertically into the free vortex and have a profound influence on its structure.

The boundary-layer flow in Region B can be thought of as producing an inward radial jet at $r = r_{up}$, the strength of which depends on the gradient wind profile at larger radii as well as on the boundary-layer depth. The boundary-layer dynamics in Region A determine the fate of this jet, but the details depend *inter alia* on the radial pressure gradient at the top of the boundary layer, i.e. there is a substantial two-way feedback between the boundary layer and the free vortex in this region. These details depend also on the boundary-layer depth. The radial pressure gradient in the boundary layer is probably still determined in large measure by the mass distribution in the free vortex, with possible exceptions in localized regions near where inflow turns to upflow
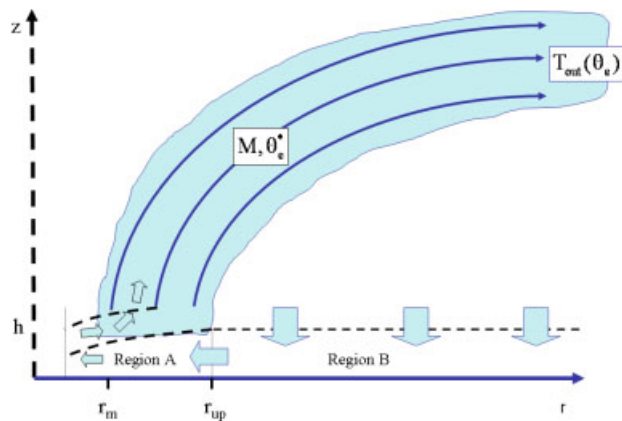

Figure 1. Conceptual model of the hurricane inner-core region proposed by Smith *et al.* (2008). Air subsides into the boundary layer for radii $r > r_{up}$ and ascends out of the boundary layer for $r < r_{up}$. The frictionally induced net pressure gradient in the outer region produces a radially inward jet at $r = r_{up}$. The subsequent evolution of this jet depends on the bulk radial pressure gradient that can be sustained by the mass distribution at the top of the boundary layer. The jet eventually generates supergradient tangential winds whereafter the radial flow rapidly decelerates and turns upwards and outwards. When the outflow has adjusted to the radial pressure gradient that is sustained by the mass field, the flow turns upwards into the eyewall clouds. This figure is available in colour online at www.interscience.wiley.com/journal/qj

and possibly outflow (section 4). However the free vortex can be expected to be strongly influenced by the radial distribution of mass, momentum and moisture that leave the boundary layer.

The slab-model boundary-layer calculations by Smith and Vogl (2008) and Smith *et al.* (2008) show that the tangential winds tend to become supergradient in the inner core and, as a result, the radial flow rapidly decelerates until the tangential component becomes subgradient again, or the radial wind becomes zero. In either case the flow out of the boundary layer increases markedly. If the winds carried upwards retain their supergradient character, they will surely flow with a significant component outwards until they have come into gradient wind adjustment with the mass field aloft. At this point they would be expected to turn upwards into the eyewall. While parts of this scenario were speculative until now, the model is consistent with flight-level and radar observations of the inner core at low levels in hurricane *Hugo* (Marks *et al.* 2008) and hurricane *Isabel* (Montgomery *et al.*, 2006b; Aberson *et al.*, 2006), and it is consistent with the calculations of Montgomery *et al.* (2001) and Persing and Montgomery (2003). The three-dimensional calculations of M1 provide a wealth of data with which to examine the azimuthally averaged aspects of the boundary-layer dynamics and the manner in which the boundary layer couples with the interior flow. One aim of the present paper is to use these data to assess the validity of the conceptual model in Figure 1.

Previous theoretical accounts of tropical cyclone evolution have presumed that convergence above the boundary layer is a prerequisite for intensification and that this convergence must be large enough to oppose the frictionally induced divergent outflow above the boundary layer (Ooyama, 1969, 1982; Willoughby, 1988, 1995;

[†]Throughout this paper we use the term *boundary layer* to describe the shallow layer of *strong* inflow near the sea surface that is typically 500 m to 1 km deep and which arises *largely* because of the frictional disruption of gradient wind balance near the surface. While in our model calculations there is some inflow throughout the lower troposphere associated with the balanced response of the vortex to latent heat release in the eyewall clouds (we show this in a paper to the *Quarterly Journal* that has been accepted subject to minor revision), the largest radial wind speeds are confined within the lowest kilometre and delineate clearly the layer in which friction effects are important (i.e. where there is gradient wind imbalance; Figure 6) from the region above where they are not.

Raymond *et al.*, 1998; Smith, 2000). In addition it has been supposed that friction generally reduces the winds in the boundary layer below the local gradient-wind value. For example, Willoughby (1995, p 29) notes that 'the swirling wind in the boundary layer is generally a little weaker than that just above' and Schubert and Alworth (1987, p 157), in their theoretical study of tropical cyclone development using a Sawyer–Eliassen balanced vortex model, state that '... one would expect that the inclusion of friction would reduce the low-level winds ... to bring closer agreement with observations'. In this connection, Kepert (2001, p 2469) has discussed the issue of estimating a surface wind reduction factor in the context of observational studies. More recently, Raymond *et al.* (1998, 2007) assume that the boundary layer is generally responsible for spin-down, noting that '... cyclone development occurs when the tendency of convergence to enhance the low-level circulation of a system defeats the tendency of surface friction to spin the system down'. The key issue here is what is being converged and where is the convergence occurring? The scenario envisaged by Raymond *et al.* is that frictionally induced convergence in the boundary layer forces deep convection, which then generates inflow through a deep tropospheric layer. In a very recent paper, Raymond and colleagues (Marin *et al.*, 2009) continue to assert that 'The primary balance governing the circulation in the planetary boundary layer is between the convergence of environmental vorticity, which tends to spin up the storm, and surface friction, which tends to spin it down'. In general, the perception seems to be that surface friction plays only an inhibiting role to vortex intensification. We argue below and later demonstrate that this is not the case in the inner-core region.

The idea that convergence above the boundary layer is a prerequisite for vortex spin-up is that, in the absence of friction, the absolute angular momentum, M, is materially conserved. This quantity is related to the tangential wind speed, v, by the formula

$$v = \frac{M}{r} - \frac{fr}{2},$$

where f is the Coriolis parameter. For constant M, both terms in this expression lead to an increase in v as r decreases. An alternative, but equivalent interpretation for the acceleration of the mean tangential wind follows directly from Newton's second law in which the sole force is the generalized Coriolis force associated with the mean radial component of inflow. (The generalized Coriolis force is $-u(v/r + f)$, where u is the mean radial velocity component.) In the boundary layer, absolute angular momentum is not materially conserved because of the frictional torque in the tangential direction. However, if rings of air converge quickly enough, i.e. if the generalized Coriolis force exceeds the tangential component of frictional force, the tangential winds can increase with decreasing radius in the boundary layer as well. It is precisely for this reason that supergradient winds can arise in the boundary layer (e.g. Nguyen *et al.*, 2002; Smith and Vogl, 2008).

The tendency for supergradient winds to develop in the boundary layer raises the possibility that the spin up of the inner core might be associated with the convergence of absolute angular momentum in the boundary layer and that it could proceed largely independently of the spin-up of the outer circulation. There is some evidence for this possibility. For example, in Emanuel's (1997, 2003) model of hurricane intensification as a frontogenetic process in equivalent potential temperature, core spin-up appears to arise entirely in the boundary layer. (Emanuel takes the boundary layer to be a layer of fixed depth in which the frictional stress is distributed uniformly with height as a body force, but he assumes that gradient wind balance exists in this layer.) However, the balanced boundary layer that forms the dynamical part of that model is forbidden from generating supergradient winds (Smith and Montgomery, 2008) so that supergradient winds *per se* might not be essential. The importance of the boundary layer to vortex spin-up finds support in unpublished calculations performed by our late colleague, Wolfgang Ulrich. Using a simple axisymmetric tropical cyclone model and performing back-trajectory calculations, he found that in all calculations examined, the ring of air associated with the maximum tangential wind speed invariably emanated from the boundary layer at some large radius from the storm axis. Numerical simulations of hurricane *Andrew* (1992) by Zhang *et al.* (2001) show further evidence for the role of the boundary layer in vortex spin-up, but these authors did not appear to realize the fundamental nature of their result. These various findings naturally raise a basic question: What are the relative roles of convergence in the boundary layer to convergence above the boundary layer in the spin-up of the mean tangential winds, both in the inner core and in the region of gales? A further aim of the present paper is to investigate this question.

The focus of this paper is largely on the dynamical aspects of the azimuthally averaged mean field evolution in two of the three-dimensional numerical experiments performed by M1. Thermodynamical aspects of the mean field evolution are discussed in a companion paper, M2, which challenges the very foundations of the WISHE mechanism itself. The paper is organized as follows. Section 2 gives a brief description of the model while section 3 describes the kinematics of vortex evolution in the model. Section 4 analyses the dynamics of vortex spin-up from an azimuthally averaged perspective in the most basic numerical experiment and section 5 examines the effects of including a representation of warm-rain processes. The concusions are presented in section 6. A short appendix details terms contributing to the azimuthally averaged absolute angular momentum budget.

2. The model configuration

The numerical experiments are carried out using a modified version of the Pennsylvania State University–National Center for Atmospheric Research fifth-generation Mesoscale Model (MM5, version 3.6; Dudhia,

1993; Grell *et al.*, 1995). The model is configured with three domains: a coarse mesh of 45 km resolution and two 2-way nested domains of 15 and 5 km resolution, respectively. The domains are square and are 5400 km, 1800 km, 600 km on each side. There are 24 σ-levels in the vertical, seven of which are below 850 mb. The calculations are performed on an f-plane centred at 20°N.

In order to keep the experiments as simple as possible, the main physics options chosen are the bulk-aerodynamic boundary-layer scheme and either the simplest explicit moisture scheme that mimics pseudo-adiabatic ascent, or a warm-rain scheme. These schemes are applied in all domains. No cumulus parametrization was used on either the coarsest or second grid. The sea surface temperature is set to a constant 27 °C. For simplicity, radiative cooling is neglected. The initial vortex is axisymmetric with a maximum tangential wind speed of 15 m s^{-1} at the surface at a radius of 135 km. The strength of the tangential wind decreases sinusoidally with height, vanishing at the top model level (50 mb). The temperature field is initialized to be in gradient wind balance with the wind field using the method described by Smith (2006). The far-field temperature and humidity are based on Jordan's Caribbean sounding (Jordan, 1958).

The vortex centre is defined as the centroid of relative vorticity at 900 mb over a circular region of 200 km radius from a 'first-guess' centre, which is determined by the minimum of the total wind speed at 900 mb. Experiment 1 is the control calculation described in M1 and Experiment 2 is the corresponding calculation with a representation of warm-rain processes.

3. Kinematics of vortex spin-up

The spin-up of the vortex in both Experiments 1 and 2 is summarized in Figure 2, which shows time series of the azimuthal-mean maximum tangential wind component, V_{max}, and the magnitude of the minimum radial component, U_{min}. Both these maxima occur at low levels, the
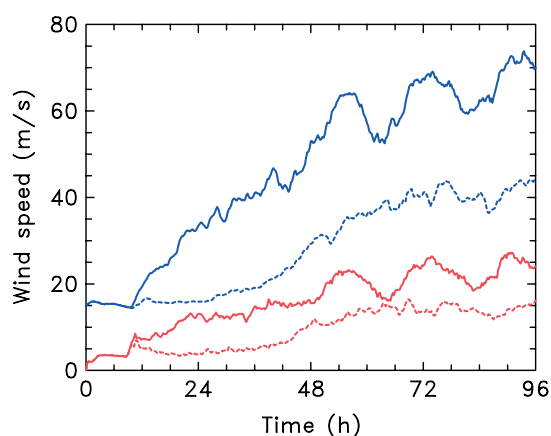

Figure 2. Vortex development in control and warm-rain experiments. Time series of azimuthal-mean maximum tangential wind component (upper two curves) and minimum radial wind component (with the sign of the radial wind reversed, lower two curves). The solid curves relate to Experiment 1, the dashed curves to Experiment 2. This figure is available in colour online at www.interscience.wiley.com/journal/qj

former at a height of a few hundred metres and the latter even lower. As in many previous numerical experiments of this type, the evolution begins with a gestation period during which the vortex slowly decays due to surface friction, but moistens in the boundary layer due to evaporation from the underlying sea surface. In these experiments, this period lasts 9 hours during which time V_{max} decreases slightly (by less than 0.5 m s^{-1}). The imposition of friction from the initial instant leads to inflow in the boundary layer and outflow above it, the outflow accounting for the slight decrease in tangential wind speed through the conservation of absolute angular momentum.

3.1. Rapid intensification and maturity

The inflow is moist and, as it rises out of the boundary layer and cools, condensation progressively occurs in some grid columns interior to the corresponding radius of maximum tangential wind speed (e.g. Smith, 1968; Smith and Vogl, 2008). Existing relative vorticity is stretched and amplified in these columns leading to the formation of localized rotating updraughts in the form of VHTs (Hendricks *et al.*, 2004; Montgomery *et al.*, 2006a). As the updraughts develop, there ensues a period lasting about 45 hours in Experiment 1 during which the mean vortex rapidly intensifies. During this time, V_{max} increases from approximately 14.5 m s^{-1} to approximately 63 m s^{-1}. The average intensification rate is approximately 1 m s^{-1} h^{-1}. After 54 hours, the intensity undergoes several marked fluctuations with a timescale of 9–12 hours while the mean intensity increases more modestly reaching approximately 70 m s^{-1} at 96 hours. In both experiments, the inflow maximum increases sharply as intensification begins. In Experiment 1 it continues to grow steadily until about 48 hours. Thereafter the maximum oscillates with a period of 12–18 hours. Significantly, the peaks and troughs in $|U_{min}|$ correlate closely with peaks and troughs in V_{max}, consistent with the role of the radial inflow in conjunction with at least the partial conservation of absolute angular momentum in the spin-up process (section 4). In Experiment 2, the maximum inflow subsides after the initial sharp increase and thereafter it slowly increases as the vortex matures. It turns out that the maximum inflow occurs in the boundary layer with speeds exceeding 25 m s^{-1} in Experiment 1 and 15 m s^{-1} in Experiment 2.

When warm-rain processes are included (Experiment 2), rapid intensification is delayed and the vortex intensifies more slowly than in the Experiment 1. The intensity at 96 hours is much lower than that in Experiment 1, the peak maximum azimuthal-mean tangential wind being approximately 45 m s^{-1} at 77 hours compared with 63 m s^{-1} at this time in Experiment 1. Experiment 2 was integrated over a longer time period than Experiment 1 to determine the final maximum intensity at this resolution. At 384 hours the maximum mean tangential wind is approximately 53 m s^{-1}. We attribute this lower maximum to a reduction in the convective instability that results from convectively driven downdraughts associated

with the rain process and from the effects of water loading, which reduces the cloud buoyancy also. The VHTs emerge from approximately 10.5 hours and are irregular and transient during the period from 12 to 36 hours. The merging and axisymmetrization processes start later than in Experiment 1 from about 36 to 60 hours.

3.2. Azimuthally averaged aspects

We consider now an azimuthal-mean perspective of the dynamics of vortex spin-up in these three-dimensional experiments. We focus for the present on Experiment 1 and begin with a description of the principal features of the flow structure and evolution. Figure 3 shows radius–height plots of the azimuthal-mean tangential wind speed and azimuthal-mean vertical component of relative vorticity at 24 and 96 hours in Experiment 1. It is noteworthy that the maximum tangential wind speed occurs at very low levels and that the vortex broadens with time as it intensifies. We have highlighted the latter feature by plotting the isotachs of gale-force ($17\,\mathrm{m\,s^{-1}}$) and hurricane-force ($33\,\mathrm{m\,s^{-1}}$) winds in Figure 3(a) and (b). Note that the radius of gales, which can be used as a measure of vortex size, and the radius of hurricane-force winds move outwards as the inner core strengthens. The progressive broadening of the vortex with time is indicated also in Figure 4(a), which shows a Hovmöller diagram of isotachs of the mean tangential

wind component at a height of 500 m. The growth rate in the radius of gales decreases from about $11\,\mathrm{km\,h^{-1}}$ during the period 24 to 36 hours to about $7\,\mathrm{km\,h^{-1}}$ during the period 84 to 96 hours. The reasons for this growth are discussed in section 4. Note that the relative vorticity is positive out to at least 250 km in Figure 3(c). The largest values occur at low levels and, at times, the maximum lies at a finite radius from the axis. Figure 4(b) shows a Hovmöller diagram of the relative vorticity at a height of 500 m. The field has been lightly smoothed by applying five passes of a 1-2-1 time filter to the data. Note that the relative vorticity has its maximum on the axis during some periods, but the maximum is mostly off the axis, especially during the later part of the calculation. This feature is even more prominent in the higher-resolution calculations summarized in M1, which used a 1.67 km horizontal grid (M1, Figure 18(d)). Note also that there is no region with negative values at this level for radii less than 250 km.

Animations of the instantaneous fields of radial and vertical motion show the presence of inertia-gravity waves initiated by the VHTs and, in order to reduce the effects of these transient flow features, it is necessary to time average the fields. Figure 5 shows radius–height cross-sections of the isotachs of the time-mean, azimuthal-mean radial velocity in the control calculation during the two-hour periods 23–25, 47–49 and 94–96 hours. It shows also the corresponding
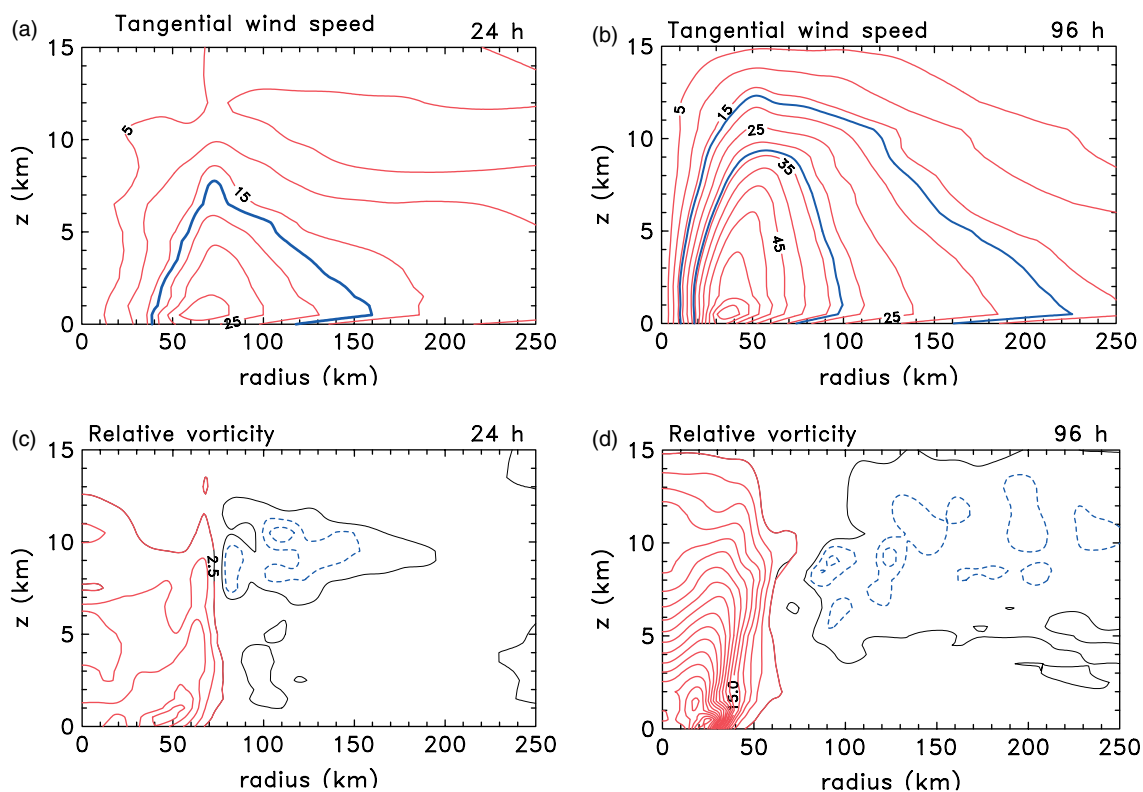

Figure 3. Radius–height cross-section of isotachs of azimuthal-mean tangential wind in the control calculation at: (a) 24, and (b) 96 hours, with contour interval $5\,\mathrm{m\,s^{-1}}$. The bold contours are those of gale-force ($17\,\mathrm{m\,s^{-1}}$) and hurricane-force ($33\,\mathrm{m\,s^{-1}}$) winds. (c) and (d) show the corresponding isopleths of the azimuthal-mean vertical component of relative vorticity, with contour interval $2.5 \times 10^{-4}\,\mathrm{s^{-1}}$ for positive values (solid) and $5 \times 10^{-5}\,\mathrm{s^{-1}}$ for negative values (dashed). The zero contour is the thin (black) line. This figure is available in colour online at www.interscience.wiley.com/journal/qj
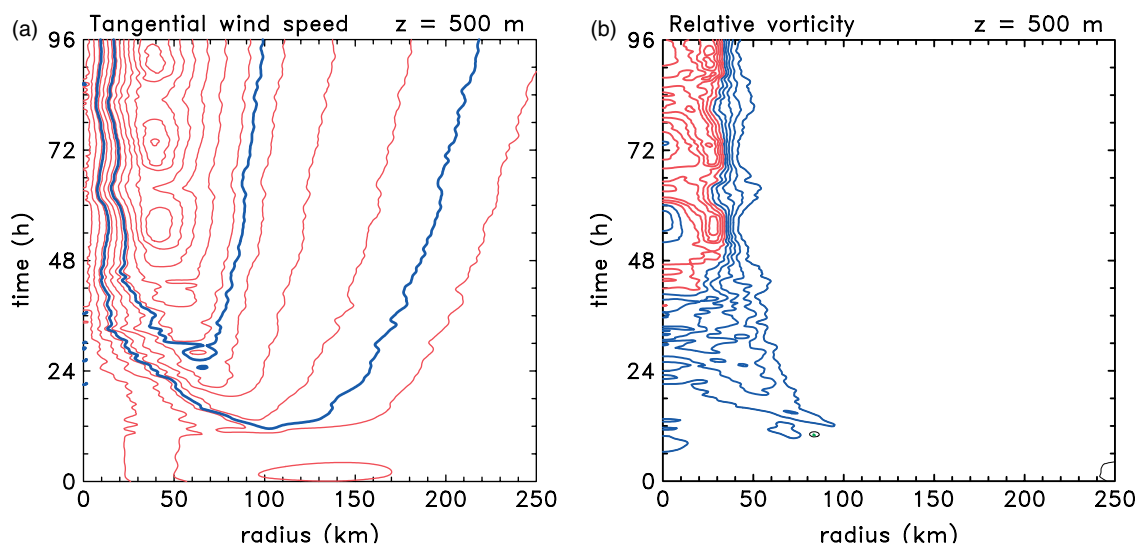
Figure 4. Hovmöller diagram of (a) isotachs of the mean tangential wind component (contour interval $5\,\mathrm{m\,s^{-1}}$), and (b) isopleths of the mean vertical component of relative vorticity (contour interval $5 \times 10^{-4}\,\mathrm{s^{-1}}$) in Experiment 1 at a height of 500 m. In (a) the bold contours show the location of gale-force ($17\,\mathrm{m\,s^{-1}}$) and hurricane-force ($33\,\mathrm{m\,s^{-1}}$) winds. In (b) the thin contours indicate values larger than $3 \times 10^{-3}\,\mathrm{s^{-1}}$ and thick contours values less than this. Note that there are no negative values at this level for the radii range shown. This figure is available in colour online at www.interscience.wiley.com/journal/qj

cross-section of the time-mean, azimuthal-mean vertical velocity during the period 94–96 hours. A notable feature is that the strongest radial inflow takes place in a very shallow boundary layer. There is generally inflow in the lower troposphere, above the boundary layer, but this is much weaker with speeds mostly less than $0.5\,\mathrm{m\,s^{-1}}$, i.e. below the lowest contour interval in Figure 5(a)–(c). At later times ((b) and (c)), there is a local region of strong outflow just above the inflow where it terminates. There is mostly outflow in the upper troposphere and this is spread over a much deeper layer than the inflow, with maxima occurring at heights of around 10 km and increasing slightly in height as the vortex intensifies. Conspicuously, there are one or two shallow regions of inflow in the upper troposphere with mean radial wind speeds reaching $2\,\mathrm{m\,s^{-1}}$. These structures, which lie adjacent to regions of strong outflow, are probably the analogues in the radial direction to the regions of subsidence that occur adjacent to strong convective plumes. They are likely associated with the occurrence of inertial instability, a speculation that requires further investigation. Also of interest is the existence of two maxima in the vertical velocity, one is low down and marks the region where the boundary-layer inflow rapidly terminates, erupting upwards and outwards (cf. Figure 1). The other maximum is located much higher and is presumably associated with the axisymmetric mean of the local buoyancy within the VHTs as documented in M2.

Figure 5(e) shows a magnified view of the structure of the three velocity components in the inner-core region averaged over the time period 94–96 hours. Noteworthy features are:

- The maximum tangential wind speed, $V_{\max}$, is located near the top of the boundary layer (defined in the footnote in section 1) at a radius of 36 km and an altitude of about 500 m.

- $V_{\max}$ is located also within the region of strongest ascent.
- A little above the location of $V_{\max}$, the flow has a large radial component outwards, the maximum exceeding $8\,\mathrm{m\,s^{-1}}$.
- The vertical velocity attains a maximum at a height of about 800 m, above which it declines, indicating that this maximum is a feature of the inertial effects in the corner region where the inflow terminates and not a result of buoyancy associated by latent heat release. This buoyancy force leads to a second vertical-velocity maximum in the middle to upper troposphere (Figure 5(d)).
- There is a narrow region of subsidence in the eye, close to the inner edge of the eyewall.

While not a central theme of this paper, it is interesting to examine the last item above in the light of a recent study by Schubert *et al.* (2007), who showed that the narrow region of subsidence in the eye occurs when the average Rossby length in the eye is less than 0.6 times the eye radius, which they took to be the radius of maximum tangential wind speed, $R_{\max}$. Schubert *et al.* (2007) defined the local Rossby length, L_R, in terms of that at large radii, say L_{RR}, which they took to be 1000 km. Specifically they defined $L_R = L_{RR}(f/I)$, where I is the the inertial stability parameter, defined as the square root of $(\zeta + f)(2v/r + f)$, where ζ is the relative vorticity. Figure 5(f) shows the radial profiles of v and L_R at a height of 1.2 km, the height of the maximum low-level subsidence rate inside the eye, for $f = 5 \times 10^{-5}\,\mathrm{s^{-1}}$, corresponding with the latitude of 20° used in the calculations here. It turns out that the average of L_R is 14 km, which is less than $0.6R_{\max}$, i.e. 24 km. Thus the narrow region of subsidence is consistent with the analytic theory of Schubert *et al.*
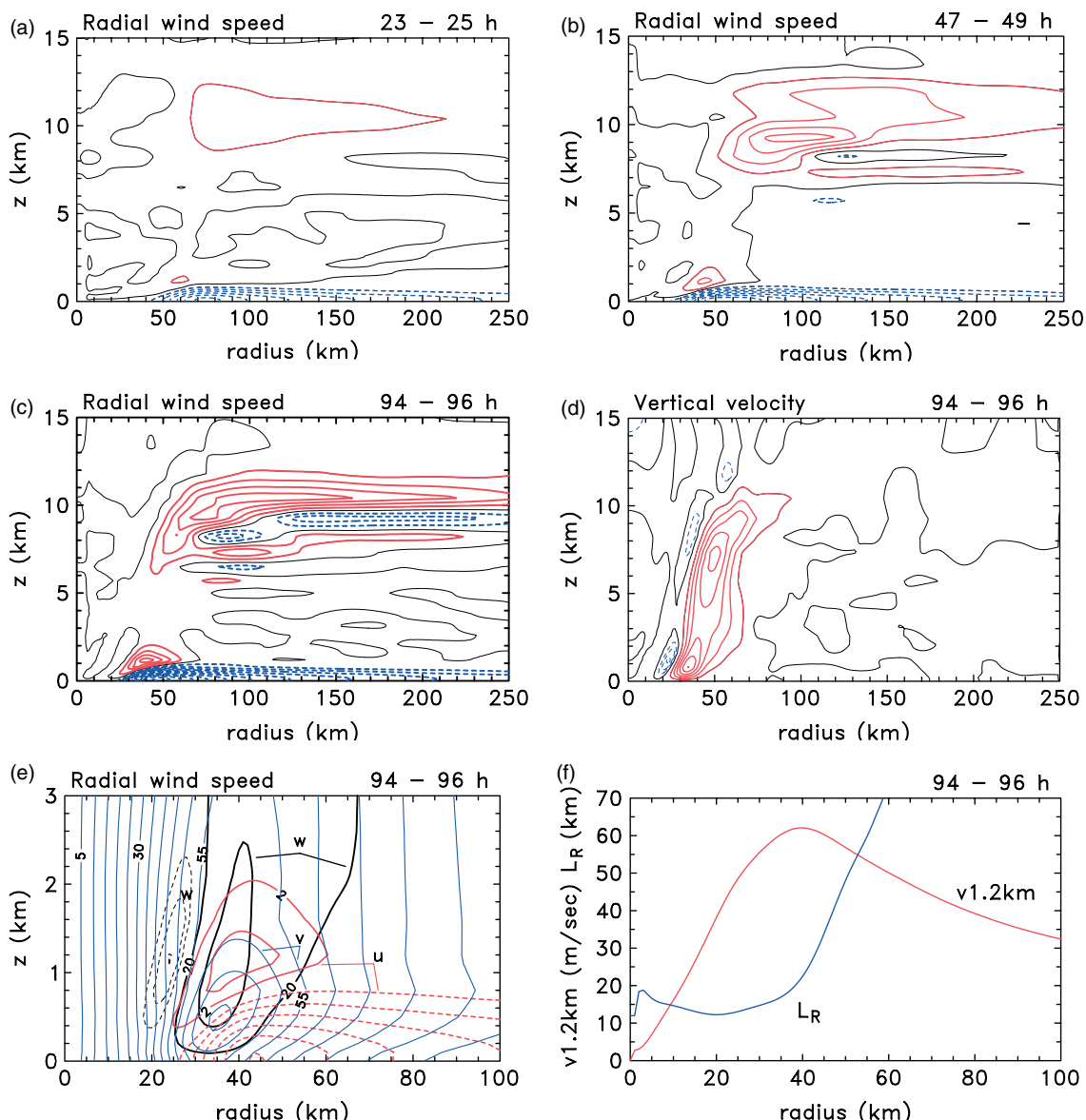
Figure 5. Radius–height cross-section of isotachs of the time-mean radial velocity in the control calculation during the periods (a) 23–25, (b) 47–49, and (c) 94–96 hours. (d) shows the corresponding cross-section for the time-mean vertical velocity during the period 94–96 hours. The contour interval in (a), (b) and (c) is $2\,\mathrm{m\,s^{-1}}$. Solid curves denote positive values, dashed curves negative values. The contour interval in (d) is $0.2\,\mathrm{m\,s^{-1}}$ for positive values and $0.04\,\mathrm{m\,s^{-1}}$ for negative values (thin dashed contours). The thin solid curve is the zero contour. (e) shows a magnified view of the contours of radial velocity (bold, marked u), tangential velocity (thin, marked v) and vertical velocity (bold black, marked w) in the inner-core region. Contours: for u, the lowest contours are $\pm 2\,\mathrm{m\,s^{-1}}$, with interval $4\,\mathrm{m\,s^{-1}}$; for v, the interval is $5\,\mathrm{m\,s^{-1}}$; for $w > 0$ the lowest contour is $0.2\,\mathrm{m\,s^{-1}}$ with interval $0.6\,\mathrm{m\,s^{-1}}$, for $w < 0$ the interval is $0.05\,\mathrm{m\,s^{-1}}$. (f) shows the radial profiles of tangential wind, v1.2km, and the estimated Rossby length, L_R, at a height of $1.2\,\mathrm{km}$ during the same time period. This figure is available in colour online at www.interscience.wiley.com/journal/qj

4. Dynamics of vortex spin-up

In the foregoing section we described kinematic aspects of the spin-up process and the mature structure of selected azimuthal mean fields. We turn now to examine the dynamical aspects, focussing special attention on the questions raised in the introduction. We consider first the revised model for the behaviour of the boundary layer in the inner-core region and its influence on the interior circulation as proposed by Smith *et al.* (2008). To this end we examine the structure of the net radial force field, F, which we define as the difference between the local radial pressure gradient and the sum of the centrifugal and Coriolis forces, i.e.

$$F = -\frac{1}{\rho}\frac{\partial p}{\partial r} + \frac{v^2}{r} + fv,$$

where p is the pressure, ρ is the air density and other quantities are as defined earlier. If $F = 0$, the tangential flow is in exact gradient wind balance; if $F < 0$, this flow is *subgradient* and if $F > 0$ it is *supergradient*.

Radius–height cross-sections of F isopleths in Experiment 1 are shown in Figure 6 at 24, 48 and 96 hours. The most prominent regions of subgradient and supergradient flow occur in the boundary layer. The flow there is
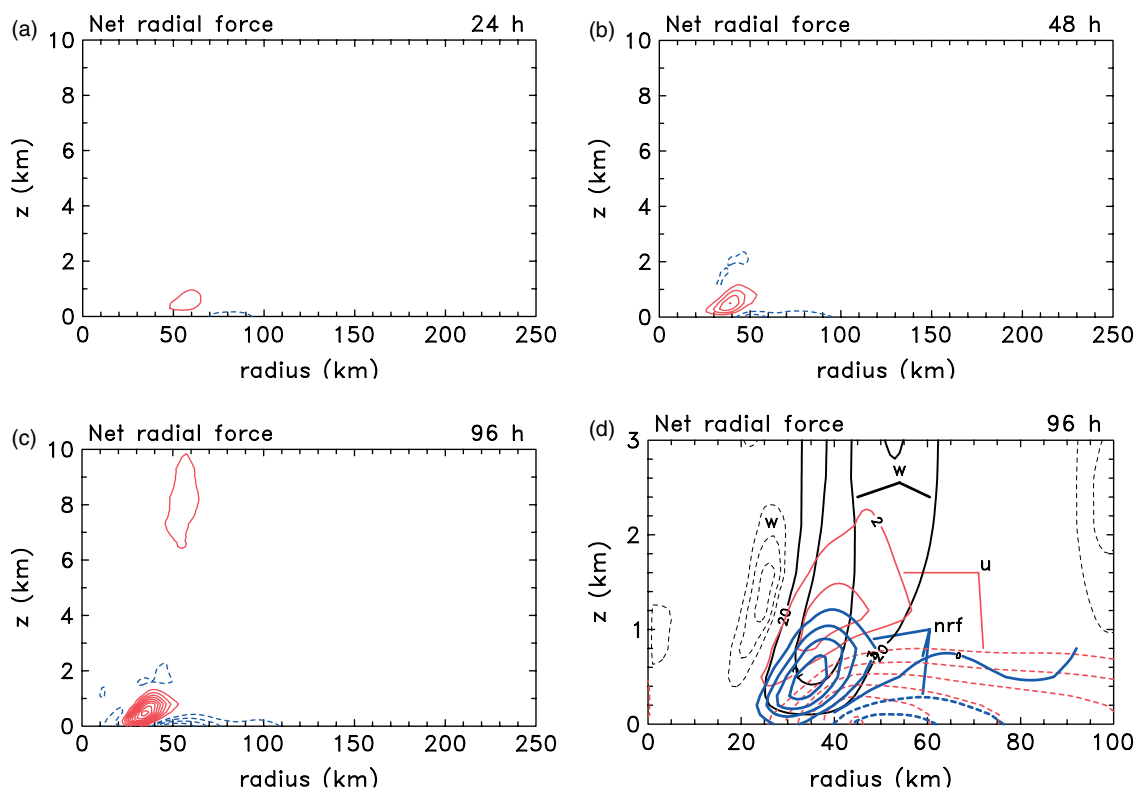
Figure 6. Radius–height cross-sections of the isopleths of the net radial force per unit mass in Experiment 1 at (a) 24, (b) 48, and (c) 96 hours. The contour interval is $1.5 \, \mathrm{m \, s^{-1} h^{-1}}$, with dashed lines indicating negative values. The zero contour is not plotted. (d) shows a magnified view of the contours of net radial force (bold, marked nrf), radial velocity (marked u) and vertical velocity (black, marked w) in the inner-core region. Contours: for u, the lowest (in magnitude) contours are $2 \, \mathrm{m \, s^{-1}}$, with interval $4 \, \mathrm{m \, s^{-1}}$; for nrf, the interval is $3 \, \mathrm{m \, s^{-1} h^{-1}}$; for $w > 0$ the lowest contour is $0.2 \, \mathrm{m \, s^{-1}}$, with interval $0.8 \, \mathrm{m \, s^{-1}}$, and for $w < 0$ the interval is $0.05 \, \mathrm{m \, s^{-1}}$. In (d) the zero contour of net radial force is plotted for $r > 40 \, \mathrm{km}$ and $z < 800 \, \mathrm{m}$ to show that the main low-level inflow coincides approximately with the region of subgradient flow. This figure is available in colour online at www.interscience.wiley.com/journal/qj

subgradient at outer radii, but it becomes *strongly* super-gradient at inner radii where the boundary layer erupts into the vortex above (cf. Figure 5(d)). As this supergradient flow is carried out of the boundary layer, it accelerates outwards, as seen in Figure 5(a)–(c), until it achieves balance with the mass field (i.e. $F \rightarrow 0$), whereupon it ascends into the eyewall, which is coincident with the column of strong vertical motion in Figure 5(d). These features are highlighted in Figure 6(d), which shows the detailed structure of the contours of net radial force in relation to the radial and vertical velocity components in the inner-core region at 96 hours. Comparison with Figure 5(e) shows clearly that the maximum tangential wind component lies in the region where the flow is supergradient. The maximum amount by which the tangential wind speed exceeds its corresponding gradient value is 23%, 14%, 22% and 18% at 24, 48, 72 and 96 hours, respectively. The eruption of the boundary layer into the vortex above at a finite radius is analogous, for example, to the flow separation that occurs in the boundary layer on an aerofoil where there is an adverse pressure gradient, the latter being equivalent to the reverse in sign of the net radial force. Figure 6 shows also that the main low-level inflow layer coincides approximately with the region of subgradient flow, indicating that the depth of the boundary layer is associated largely with the breakdown of gradient wind balance by friction.

The above features are exactly those hypothesized by Smith *et al.* (2008) for the flow behaviour in the inner core of a hurricane (Figure 1) and they are supported by observations. In particular, they provide an explanation for the observation of a skirt of moderate to high radar reflectivity adjacent to the main eyewall (e.g. Figures 5–7 of Aberson *et al.*, 2006; Figure 3 of Marks *et al.*, 2008), but still within the 'visible' eye defined by the upper-tropospheric boundary of clear and cloudy air seen in high-resolution satellite imagery (e.g. Figure 2 of Bell and Montgomery, 2008).

We address now the question: what are the relative roles of convergence in the boundary layer to convergence above the boundary layer in the spin-up of the mean tangential winds, both in the inner core and in the region of gales?

A well-known result from the inviscid axisymmetric balanced theory of vortex intensification is that the latent heat release in eyewall convection tends to produce a secondary circulation in which the tangential wind tendency is largest just inside the radius of maximum tangential wind speed (Shapiro and Willoughby, 1982, p 389). Thus in this theory the vortex tends to contract as it intensifies. An implicit assumption of this theory is that the convergence of absolute angular momentum takes place in a region above the boundary layer where this quantity is conserved and that the spin-up occurs there.

However, in the present calculations the largest tangential wind speeds and tendencies are found at low levels in the boundary layer and as a result are significantly affected by gradient wind imbalance (e.g. Figures 5(e), 6(d) and 8). Thus a balanced theory would not apply in this layer (Smith and Montgomery, 2008).

Further insight into the foregoing question is provided by an analysis of the evolution of the mean absolute angular momentum fields. Figure 7 shows radius–height plots of these fields at the initial time and at 24, 48 and 96 hours in Experiment 1. Some contours values have been plotted as thick (blue) curves to highlight specific aspects of the evolution. Following these contours is useful because, in the absence of friction, absolute angular momentum is a materially conserved property in an axisymmetric mean sense, provided at least that the

eddy fluxes associated with asymmetric motions can be ignored. We show in an appendix that this assumption is valid throughout much of the free atmosphere, the exception being in the inner core where vortical hot towers are active. Whether or not absolute angular momentum is conserved, the tangential wind speed will increase where the mean absolute angular momentum isopleths move inwards, and it will decrease where they move outwards.

4.1. Inner core spin-up

Consider first the two inner thick (blue) contours in Figure 7(a). These move inwards in the lower troposphere and outwards in the upper troposphere. It is evident that they emanate from the region where the boundary layer erupts into the vortex above and where the boundary-layer winds are supergradient (Figures 5(d) and 6). Figure 7(e)
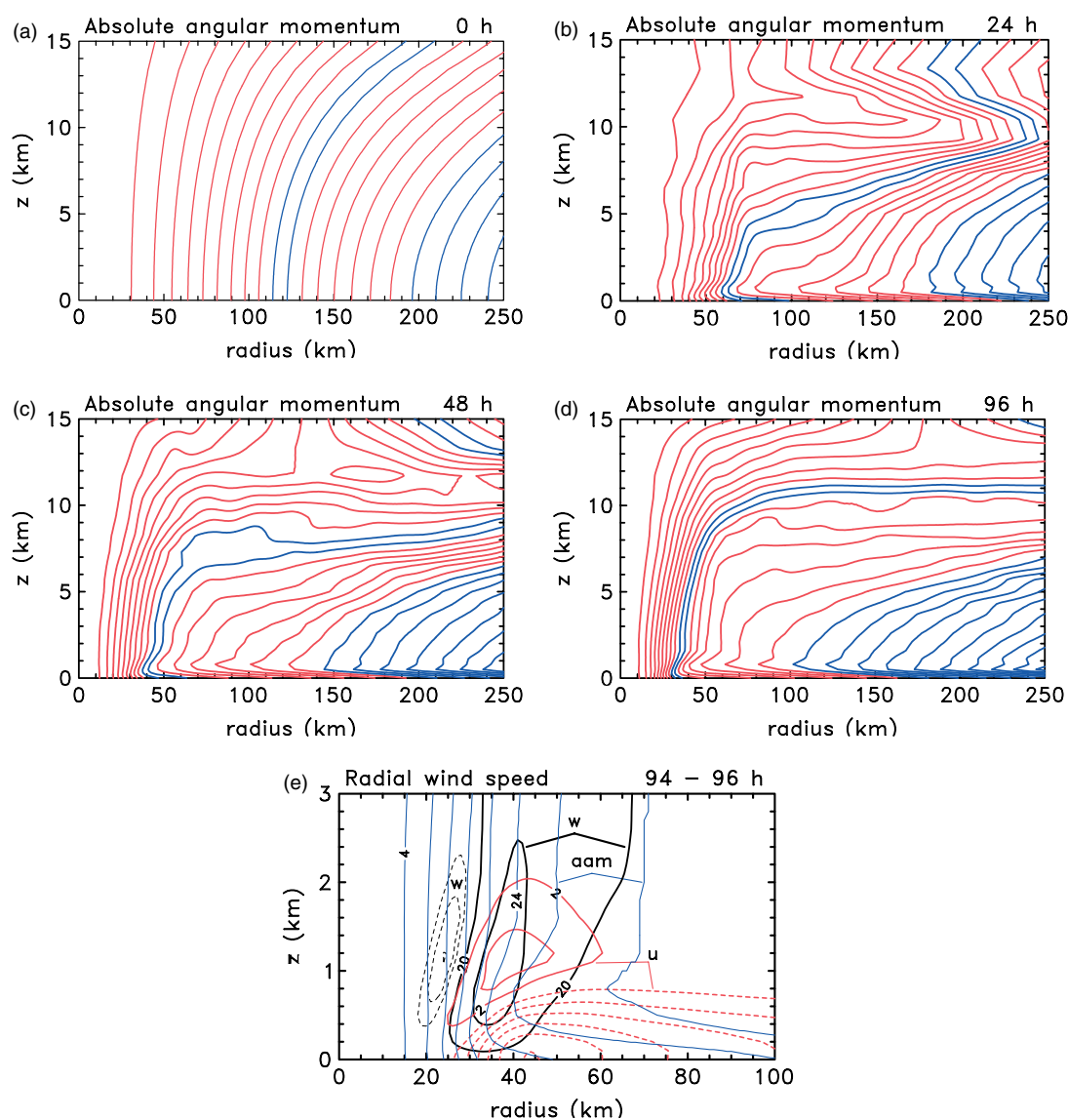

Figure 7. Radius–height cross-section of isopleths of absolute angular momentum in the control calculation at (a) the initial time, and at (b) 24, (c) 48, and (d) 96 hours. The contour interval is 2×10^5 m^{2}s^{-1}. Contours with values 2×10^6 and 2.2×10^6 m^{2}s^{-1} and those larger than 3.6×10^7 m^{2}s^{-1} are highlighted as thickened (blue) curves. (e) shows a magnified view of the contours of radial velocity (bold, marked u), absolute angular momentum (thin, marked aam) and vertical velocity (black, marked w) in the inner-core region. Contours: for u, the lowest contours are ± 2 m s^{-1} in value, with interval 4 m s^{-1}; for aam, the interval is 4×10^5 m^{2}s^{-1}; for $w > 0$ the lowest contour is 0.2 m s^{-1}, with interval 0.6 m s^{-1}; for $w < 0$, the interval is 0.05 m s^{-1}. This figure is available in colour online at www.interscience.wiley.com/journal/qj
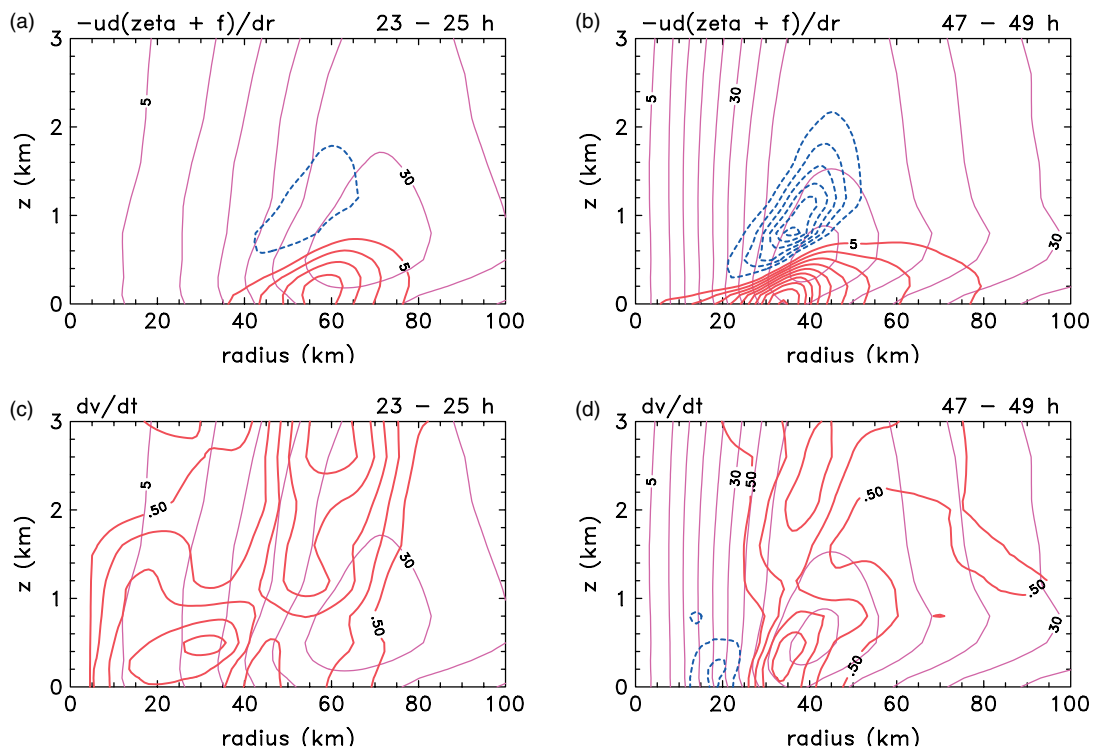
Figure 8. Radius–height cross-section of the isopleths of tangential wind tendency associated with radial advection, $-u(\zeta + f)$, in the control calculation averaged during the periods (a) 23–25 hours, and (b) 47–49 hours. The contour interval is $5\,\mathrm{m\,s^{-1}h^{-1}}$, bold curves are positive, and dashed curves negative. (c) and (d) show the total tendency, $\partial v/\partial t$, during the two time periods, with contour interval $0.5\,\mathrm{m\,s^{-1}h^{-1}}$. In all panels, the isotachs of mean tangential wind during each period are also shown, as thin solid curves, with contour interval $5\,\mathrm{m\,s^{-1}}$. This figure is available in colour online at www.interscience.wiley.com/journal/qj

shows a magnified view of the structure of the absolute angular momentum contours in the inner-core region superimposed on those of radial velocity and vertical velocity. The fields are averaged over the time period 94–96 hours. Noteworthy features are:

- The absolute angular momentum contours have a small angle to the horizontal at low levels (below 500 m) where the radial inflow is strong, consistent with strong radial advection in the presence of some diffusion to the surface.
- The largest inward displacement of a particular contour is located near the top of the inflow layer, where diffusive effects are weakest.
- The contours are nearly vertical where the radial flow is weak, e.g. above 2 km and inside a radius of 24 km.
- The contours slope upwards and outwards in the region immediately above the inflow layer where the flow is upward and outward, consistent with the material conservation of absolute angular momentum in this region.

The above results suggest an important modification of Shapiro and Willoughby's balanced picture as foreshadowed by Smith and Vogl (2008). If the boundary layer tends to generate tangential wind speeds that are larger than the existing tangential wind speed maximum above the boundary layer, and if these winds are advected vertically out of the boundary layer, they would contribute in a similar way to a spin-up of the core

region in the free atmosphere. Nevertheless, since the strongest winds occur in the boundary layer, we would expect their evolution to be tied to the pressure gradients associated with the mass distribution above the boundary layer. In summary, the intensification of the inner core is a low-level process tied strongly to the dynamics of the boundary layer, which, intrinsically, is not in gradient-wind balance.

The veracity of the foregoing ideas is exemplified by radius–height plots of the tangential wind tendency[‡], $\partial v/\partial t$, and the contribution thereto associated with radial advection, $-u(\zeta + f)$, averaged during the periods 23–25 and 47–49 hours shown in Figure 8. The domain shown is similar to that in Figures 5(e), 6(d) and 7(e). Note that during both time periods (Figure 8(a) and (b)), the maximum tendency associated with radial advection lies at low levels, especially during the period 47–49 hours. This feature is consistent with the boundary layer playing the central role in the spin-up of the inner core region. While the values shown may seem large ($23\,\mathrm{m\,s^{-1}h^{-1}}$ between 23 and 25 hours, and $50\,\mathrm{m\,s^{-1}}\ \mathrm{h^{-1}}$ between 47 and 49 hours), one must remember that these tendencies are opposed by surface friction and vertical advection so that the net tendencies are much smaller with maxima on the order of $2\text{–}3\,\mathrm{m\,s^{-1}h^{-1}}$ (see Figure 8(c) and (d), noting that the contour interval is only one tenth

---

[‡]The tendencies were calculated as centred time differences from MM5 output of azimuthally-averaged tangential wind data every 15 minutes.

of that in (a) and (b)). Moreover, these maxima do not coincide with the actual location of the maximum tangential wind speed so that the actual increases in the maximum wind speed are even smaller still.

4.2. A thought experiment

One way of thinking about the role of the boundary layer is to imagine imposing an annular elevated heating distribution, first in an initially neutrally stratified non-rotating fluid. The buoyancy force produced by the heating will drive a vertical circulation and the induced low pressure beneath the heat source will produce convergence from inside and outside the annulus, irrespective of the presence of friction at the lower boundary (e.g. Smith *et al.*, 2005, section 7). Now assume that the fluid is rotating about a vertical axis and that there is a frictional boundary layer. The inertial stability of the vortex will impede the ability of the low-level pressure gradient induced by the heat source to produce convergence, since as fluid converges conserving its absolute angular momentum, it will spin faster and the outward-directed centrifugal and Coriolis forces acting on the tangential flow will progressively increase and steadily move towards balance with the radial pressure gradient. However, in the presence of surface friction, the tangential flow will be reduced, as will the centrifugal and Coriolis forces, but the radial pressure gradient remains largely unchanged. The result is a net radial force in a shallow boundary layer. This force produces radial convergence and will drive inflow: we may think of it as producing a shallow radial inflow jet (Smith and Vogl, 2008). This jet will break the symmetry between fluid converging from both inner and outer radii towards the annulus of heating, favouring flow from outside. If the radial jet is strong, it may overshoot underneath the heat source before ascending, together with some of the flow converging outwards from inside the annulus, into the annulus itself.

The fate of the jet as it approaches the heat source is determined by boundary-layer dynamics, except perhaps within one or two boundary-layer depths of the heat source itself, where the vertical perturbation pressure gradient becomes important in deflecting the inflow into the upflow within the annulus. (Recall that boundary-layer theory assumes that the perturbation pressure gradient normal to the boundary can be ignored.) Although a fraction of the absolute angular momentum of the converging flow is lost by the tangential component of friction, the tangential velocity of fluid parcels continues to increase as they move inwards (section 1). What happens in the numerical experiments described above is that, eventually, the tangential wind becomes so large that the centrifugal and Coriolis forces exceed the local radial pressure gradient induced by the heat source and the jet suffers rapid deceleration, just as a rising convective updraught undergoes rapid deceleration after it punches through the tropopause and enters the very stable stratosphere. The strong inward deceleration is accompanied by a strong upflow (which must be associated with a large perturbation pressure gradient) that carries the rapidly rotating (supergradient) flow above the inflow layer where it is able to flow outwards. As it does so, conserving its absolute angular momentum, it spins more slowly and progressively achieves gradient wind balance as it rises in the updraught produced by the heating.

The main difference between the present numerical experiments and the thought experiment is that, in the former, the location of the heating is not prescribed, but determined as part of the solution. The unbalanced dynamics in the overshoot region are important in determining the maximum radial and tangential flow speeds that can be attained, and hence are important in determining the azimuthal-mean intensity of the vortex.

4.3. Outer core spin-up

Let us consider now the outer thick (blue) contours in Figure 7(a). It is clear that these move steadily inwards, but they lie above the region where the boundary-layer winds are subgradient and where the flow is subsiding into the boundary layer (e.g. Figure 7(d)). The inward motion is to be expected from the plots of mean radial motion shown in Figure 5(a)–(c). This slow but progressive inward motion explains the spin-up of the outer circulation. (It is shown in the appendix that absolute angular momentum is closely conserved in this region.) As the radial motion and spin-up occur in a region above the boundary layer where the tangential flow is close to gradient wind balance, it may be readily interpreted as resulting from the balanced response of the flow to gradual changes in the azimuthally averaged heating rate in the convective region of the vortex. Such a response is described approximately by the Sawyer–Eliassen equation (Willoughby, 1979; Shapiro and Willoughby, 1982; Smith *et al.*, 2005; Montgomery *et al.*, 2006a), a matter that will be investigated in a forthcoming paper.

The above results provide a possible physical explanation for certain long-standing observations of typhoons by Weatherford and Gray (1988), which indicate that inner-core changes in the azimuthal-mean tangential wind speed often occur independently from those in the outer core. (These authors define the inner core as the region from the storm centre to a radius of 111 km, or 1° latitude, and the outer core as the radial distance 111 to 278 km, or 2.5° latitude). We have shown that there are two largely independent mechanisms for bringing about such wind-speed changes, one of them that serves to intensify the core and the other that acts to spin up the outer circulation. We say *largely* because any change in the outer circulation above the boundary layer will have an effect also on the boundary-layer inflow. A quantification of this effect using a simple slab boundary-layer model is given by Smith *et al.* (2008, Figure 5 therein).

5. The effects of warm rain

The foregoing features of the control calculation are all present in the calculation with warm rain, the principal difference being that the secondary circulation in this case is weaker, consistent with a weaker vortex (Figure 1).

To illustrate this fact we show in Figure 9 the fields in the warm-rain calculation corresponding to those in Figures 5(c, d), 6(c), and 7(d), respectively. The azimuthal-mean radial flow shows again strong inflow in a shallow boundary layer with a localized region of strong outflow just above the inflow layer in the inner core (Figure 8(a)). This outflow feeds into the eyewall updraught (Figure 9(b)). The main outflow in the upper troposphere extends over a layer about 1.5 km deep centred at a little over 10 km in height at large radii, the maximum speed being about $2-3\,\mathrm{m\,s^{-1}}$. Below the outflow layer is a region of weak (less than $1\,\mathrm{m\,s^{-1}}$) inflow that slopes downward with decreasing radius. The mean eyewall updraught is considerably weaker than in Experiment 1 (compare Figure 9(b) with Figure 5(d)), but again shows two maxima, one at low levels and the other in the middle troposphere. Moreover, the net radial force is inward in the boundary layer except in the inner core, where it becomes strong and outward corresponding to supergradient flow (Figure 9(c)). The absolute angular momentum field is similar also to that in Experiment 1, but the inward displacement of the contours is less, consistent, of course, with the weaker vortex (compare Figure 9(d) with Figure 7(d)).

6. Conclusions

We have revisited the problem of interpreting the dynamics of tropical cyclone intensification in a three-dimensional numerical model in an axisymmetric framework. In particular we have identified two independent mechanisms for vortex intensification in this framework, both involving the radial convergence of absolute angular momentum.

- The first mechanism is associated with radial convergence *above the boundary layer* in conjunction with the conservation of absolute angular momentum. The convergence is produced by increasing system-scale radial buoyancy gradients associated with deep, inner-core convection in the presence of enhanced surface moisture fluxes. This mechanism has been articulated previously by many authors. It explains why the vortex expands in size and may be interpreted in terms of balanced dynamics.
- The second mechanism is associated with radial convergence *within the boundary layer* and becomes important in the inner core. It is likely to be enhanced by the development of supergradient winds there. Although absolute angular momentum is not materially conserved in the boundary layer, large wind speeds can be achieved if the radial inflow is sufficiently large to bring the air parcels to small radii with minimal loss of angular momentum. This mechanism is tied fundamentally to the dynamics of the boundary layer, where the flow is not in gradient-wind balance.

The existence of these two mechanisms provides a plausible physical explanation for certain long-standing
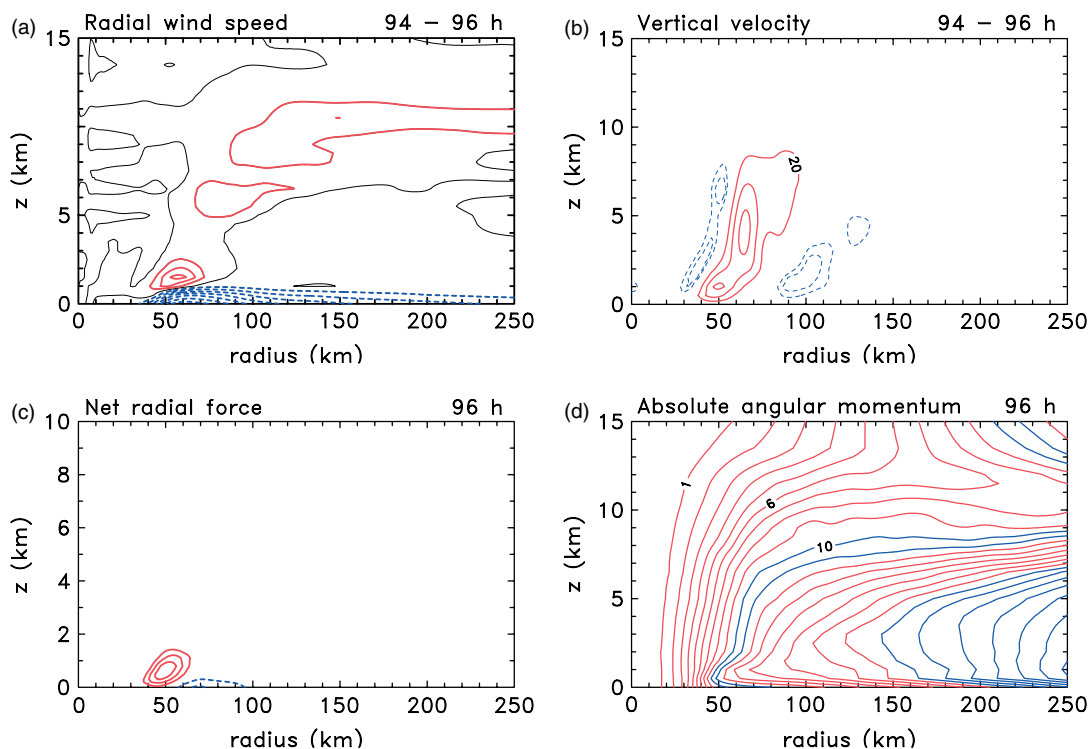

Figure 9. Radius–height cross-sections of isopleths in the warm-rain calculation at 96 hours: (a) radial velocity (contour interval $2\,\mathrm{m\,s^{-1}}$; positive bold solid and negative dashed, with thin zero line); (b) vertical velocity (contour interval $20\,\mathrm{cm\,s^{-1}}$ for positive (solid) values and $2\,\mathrm{cm\,s^{-1}}$ for negative (dashed) values); (c) net radial force (contour interval $1.5\,\mathrm{m\,s^{-1}\,h^{-1}}$, with solid curves indicating positive values, dashed curves negative values; zero contours are not shown); (d) absolute angular momentum (contour interval $1 \times 10^6\,\mathrm{m^2\,s^{-1}}$). These figures should be compared with Figures 5(c, d), 6(c) and 7(d), respectively. This figure is available in colour online at www.interscience.wiley.com/journal/qj

observations of typhoons by Weatherford and Gray, which indicate that inner-core changes in the azimuthal-mean tangential wind speed often occur independently from those in the outer core.

Where the tangential winds become supergradient, the boundary-layer inflow is rapidly decelerated and the supergradient winds are carried upwards and outwards to feed into the eyewall clouds. The region of outward radial flow immediately above the shallow inflow in the boundary layer supports the hypothesis encapsulated in Figure 1 concerning the flow structure in this region. A simple thought experiment was presented to illustrate the role and importance of the unbalanced dynamics in the inner-core region in determining the maximum radial and tangential flow speeds that can be ultimately attained in the vortex. Indeed, we have sought to highlight the importance of gradient-wind imbalance in the boundary layer in determining the azimuthal-mean intensity of the vortex, both in the numerical simulations and in reality.

An interesting question is whether the spin-up process predicted by Emanuel's (1997, 2003) theory of eyewall frontogenesis accurately or even qualitatively captures the spin-up behaviour of *both* the inner core *and* the outer circulation as presented here. This question remains a topic for further investigation.

What we have not done in this paper is to relate the boundary-layer convergence to the buoyant forcing of the vortex aloft and to the constraints on the convergence therein imposed by the boundary-layer dynamics. The latter constraints depend on the tangential wind profiles above the boundary layer where the air is subsiding into it and these profiles, in turn, are determined by the convergence of absolute angular momentum above the boundary layer in response to convective heating in the core region. A theory that brings all these constraints together to form a comprehensive theory of tropical cyclone evolution has still to be worked out, but such a theory is necessary, for example, for constructing an improved theory for the potential intensity of a tropical cyclone.

Appendix
The absolute angular momentum budget

To examine the extent to which the azimuthally averaged absolute angular momentum is conserved in the foregoing calculations (section 4), it is appropriate to investigate the absolute angular momentum budget. The absolute angular momentum, M, is defined by

$$M = rv + \frac{1}{2}fr^2,$$

where r is the radius, v is the tangential wind speed, and f is the Coriolis parameter. For axisymmetric flow it satisfies the equation

$$\frac{\partial M}{\partial t} + u\frac{\partial M}{\partial r} + w\frac{\partial M}{\partial z} = F, \qquad (A.1)$$

where F represents the frictional torque and eddy angular momentum source. Equation (A.1) implies that for
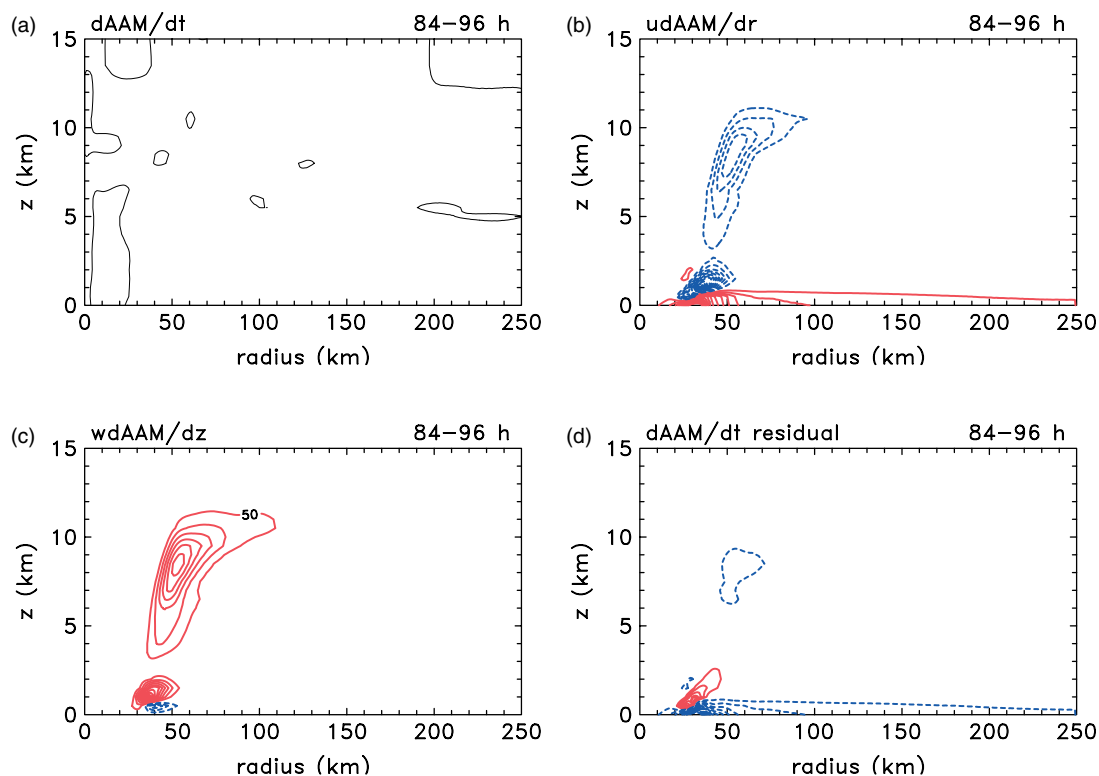

Figure A.1. Radius–height cross-sections of (a) the absolute angular momentum tendency, and the contributions to this tendency from the (b) radial, and (c) vertical advection, during the period 84 to 96 hours in Experiment 1. (d) shows the residual contribution, assumed to be largely associated with frictional effects. The contour interval is $50\,\mathrm{m^2s^{-2}}$, and solid lines indicate gain and dashed lines loss of absolute angular momentum. This figure is available in colour online at www.interscience.wiley.com/journal/qj

frictionless axisymmetric flow ($F = 0$), M is materially conserved. Height–radius cross-sections of the terms in this equation averaged during the period 84 to 96 hours in Experiment 1 are shown in Figure A.1. The radial and vertical advective tendencies, $u(\partial M/\partial r)$ and $w(\partial M/\partial z)$ make the largest contributions to the time tendency, $\partial M/\partial t$, and they almost cancel. The frictional and eddy source term F, estimated here as a residual, makes an important contribution in the boundary layer as expected and also a slight contribution in the eyewall region, presumably a reflection of eddy activity in the inner core region associated with the VHTs.

Acknowledgements

References

Aberson SD, Montgomery MT, Bell MM, Black ML. 2006. Hurricane Isabel (2003): New insights into the physics of intense storms. Part II – Extreme localized wind. *Bull. Am. Meteorol. Soc.* **87**: 1349–1357.

Asnani GC. 2005. *Tropical Meteorology*, revised edition. Pune: India.

Bell MM, Montgomery MT. 2008. Observed structure, evolution, and potential intensity of Category 5 Hurricane Isabel (2003) from 12 to 14 September. *Mon. Weather Rev.* **65**: 2025–2046.

Bister M, Emanuel KA. 1998. Dissipative heating and hurricane intensity. *Meteorol. Atmos. Phys.* **65**: 233–240.

Craig GC, Gray SL. 1996. CISK or WISHE as a mechanism for tropical cyclone intensification. *J. Atmos. Sci.* **53**: 3528–3540.

Dudhia J. 1993. A non-hydrostatic version of the Penn State–NCAR mesoscale model: Validation tests and simulation of an Atlantic cyclone and cold front. *Mon. Weather Rev.* **121**: 1493–1513.

Emanuel KA. 1988. The maximum intensity of hurricanes. *J. Atmos. Sci.* **45**: 1143–1155.

Emanuel KA. 1995. Sensitivity of tropical cyclones to surface exchange coefficients and a revised steady-state model incorporating eye dynamics. *J. Atmos. Sci.* **52**: 3969–3976.

Emanuel KA. 1997. Some aspects of hurricane inner-core dynamics and energetics. *J. Atmos. Sci.* **54**: 1014–1026.

Emanuel KA. 2003. Tropical Cyclones. *Annu. Rev. Earth Planet. Sci.* **31**: 75–104.

Emanuel KA, Neelin JD, Bretherton CS. 1994. On large-scale circulations in convecting atmospheres. *Q. J. R. Meteorol. Soc.* **120**: 1111–1144.

Grell GA, Dudhia J, Stauffer DR. 1995. A description of the fifth generation Penn State/NCAR mesoscale model (MM5). Tech Note NCAR/TN-398+STR. NCAR: Boulder. http://www.mmm.ucar.edu/mm5/documents/mm5-desc-doc.html

Hendricks EA, Montgomery MT, Davis CA. 2004. On the role of 'vortical' hot towers in formation of tropical cyclone Diana (1984). *J. Atmos. Sci.* **61**: 1209–1232.

Holton JR. 2004. *An introduction to dynamic meteorology.* Academic Press: London.

Houze RA, Chen SS, Smull BF, Lee W-C, Bell MM. 2007. Hurricane intensity and eyewall replacement. *Science* **315**: 1235–1239.

Jordan CL. 1958. Mean soundings for the West Indies area. *J. Meteorol.* **15**: 91–97.

Kepert JD. 2001. The dynamics of boundary layer jets within the tropical cyclone core. Part I: Linear Theory. *J. Atmos. Sci.* **58**: 2469–2484.

Kepert JD, Wang Y. 2001. The dynamics of boundary layer jets within the tropical cyclone core. Part II: Nonlinear enhancement. *J. Atmos. Sci.* **58**: 2485–2501.

Lighthill MJ. 1998. Fluid mechanics of tropical cyclones. *Theoret. Comput. Fluid. Dyn.* **10**: 321.

Marin JC, Raymond DJ, Raga GB. 2009. Intensification of tropical cyclones in the GFS model. *Atmos. Chem. Phys.* **9**: 1407–1417.

Marks FD, Black PG, Montgomery MT, Burpee RW. 2008. Structure of the eye and eyewall of hurricane Hugo (1989). *Mon. Weather Rev.* 1237–1259.

Molinari J, Vollaro D, Corbosiero KL. 2004. Tropical cyclone formation in a sheared enviroment: A case study. *J. Atmos. Sci.* **61**: 2493–2509.

Montgomery MT, Snell HD, Yang Z. 2001. Axisymmetric spindown dynamics of hurricane-like vortices. *J. Atmos. Sci.* **58**: 421–435.

Montgomery MT, Nicholls ME, Cram TA, Saunders AB. 2006a. A vortical hot tower route to tropical cyclogenesis. *J. Atmos. Sci.* **63**: 355–386.

Montgomery MT, Bell MM, Aberson SD, Black ML. 2006b. Hurricane Isabel (2003): New insights into the physics of intense storms. Part I – Mean vortex structure and maximum intensity estimates. *Bull. Am. Meteorol. Soc.* **87**: 1335–1348.

Montgomery MT, Nguyen SV, Smith RK. 2009. Do tropical cyclones intensify by WISHE?. *Q. J. R. Meteorol. Soc.* in press.

Nguyen CM, Smith RK, Zhu H, Ulrich W. 2002. A minimal axisymmetric hurricane model. *Q. J. R. Meteorol. Soc.* **128**: 2641–2661.

Nguyen SV, Smith RK, Montgomery MT. 2008. Tropical-cyclone intensification and predictability in three dimensions. *Q. J. R. Meteorol. Soc.* **134**: 563–582.

Ooyama KV. 1969. Numerical simulation of the life cycle of tropical cyclones. *J. Atmos. Sci.* **26**: 3–40.

Ooyama KV. 1982. Conceptual evolution of the theory and modeling of the tropical cyclone. *J. Meteorol. Soc. Japan* **60**: 369–380.

Persing J, Montgomery MT. 2003. Hurricane superintensity. *J. Atmos. Sci.* **60**: 2349–2371.

Raymond DJ, López-Carrillo C, López Cavazos L. 1998. Case-studies of developing east Pacific easterly waves. *Q. J. R. Meteorol. Soc.* **124**: 2005–2034.

Raymond DJ, Sessions SL, Fuchs Z. 2007. A theory for the spin-up of tropical depressions. *Q. J. R. Meteorol. Soc.* **133**: 1743–1754.

Schubert WH, Alworth BT. 1987. Evolution of potential vorticity in tropical cyclones. *Q. J. R. Meteorol. Soc.* **113**: 147–162.

Schubert WH, Rozoff CM, Vigh JL, McNoldy BD, Kossin JP. 2007. On the distribution of subsidence in the hurricane eye. *Q. J. R. Meteorol. Soc.* **133**: 1–20.

Shapiro LJ. 1983. The asymmetric boundary layer under a translating hurricane. *J. Atmos. Sci.* **40**: 1984–1998.

Shapiro LJ, Willoughby H. 1982. The response of balanced hurricanes to local sources of heat and momentum. *J. Atmos. Sci.* **39**: 378–394.

Smith RK. 1968. The surface boundary layer of a hurricane. *Tellus* **20**: 473–484.

Smith RK. 2003. A simple model of the hurricane boundary layer. *Q. J. R. Meteorol. Soc.* **129**: 1007–1027.

Smith RK. 2000. The role of cumulus convection in hurricanes and its representation in hurricane models. *Rev. Geophys.* **38**: 465–489.

Smith RK. 2006. Accurate determination of a balanced axisymmetric vortex. *Tellus* **58A**: 98–103.

Smith RK, Montgomery MT. 2008. Balanced boundary layers in hurricane models. *Q. J. R. Meteorol. Soc.* **134**: 1385–1395.

Smith RK, Vogl S. 2008. A simple model of the hurricane boundary layer revisited. *Q. J. R. Meteorol. Soc.* **134**: 337–351.

Smith RK, Montgomery MT, Zhu H. 2005. Buoyancy in tropical cyclones and other rapidly rotating atmospheric vortices. *Dyn. Atmos. Oceans* **40**: 189–208.

Smith RK, Montgomery MT, Vogl S. 2008. A critique of Emanuel's hurricane model and potential intensity theory. *Q. J. R. Meteorol. Soc.* **134**: 551–561.

Terwey WD, Montgomery MT. 2008. Secondary eyewall formation in two idealized, full-physics modeled hurricanes. *J. Geophys. Res.* **113**: D12112. DOI: 10.1029/2007JD008897

Weatherford CL, Gray WM. 1988. Typhoon structure as revealed by aircraft reconnaissance. Part I. Data analysis and climatology. *Mon. Weather Rev.* **116**: 1032–1043.

Willoughby HE. 1979. Forced secondary circulations in hurricanes. *J. Geophys. Res.* **84**: 3173–3183.

Willoughby HE. 1988. The dynamics of the tropical cyclone core. *Aust. Meteorol. Mag.* **36**: 183–191.

Willoughby HE. 1995. Mature structure and evolution. Pp 21–62 in *Global Perspectives on Tropical Cyclones*. WMO/TD-No. 693, Elsberry RL. (ed.) World Meteorological Organization: Geneva.

Yano J-I, Emanuel KA. 1991. An improved model of the equatorial troposphere and its coupling with the stratosphere. *J. Atmos. Sci.* **48**: 377–389.

Zhang D-L, Liu Y, Yau MK. 2001. A multi-scale numerical study of hurricane Andrew (1992). Part IV: Unbalanced flows. *Mon. Weather Rev.* **129**: 92–107.